Superfluorescence from photoexcited semiconductor quantum wells: Magnetic field, temperature, and excitation power dependence

Kankan Cong,[1] Yongrui Wang,[2] Ji-Hee Kim,[1,*] G. Timothy Noe II,[1] Stephen A. McGill,[3]
Alexey Belyanin,[2] and Junichiro Kono[1,4,5,†]

[1]*Department of Electrical and Computer Engineering, Rice University, Houston, Texas 77005, USA*
[2]*Department of Physics and Astronomy, Texas A&M University, College Station, Texas 77843, USA*
[3]*National High Magnetic Field Laboratory, Tallahassee, Florida 32310, USA*
[4]*Department of Physics and Astronomy, Rice University, Houston, Texas 77005, USA*
[5]*Department of Materials Science and NanoEngineering, Rice University, Houston, Texas 77005, USA*

Superfluorescence (SF) is a many-body process in which a macroscopic polarization spontaneously builds up from an initially incoherent ensemble of excited dipoles and then cooperatively decays, producing a delayed pulse of coherent radiation. SF arising from electron-hole recombination has recently been observed in $In_{0.2}Ga_{0.8}As$/GaAs quantum wells [G. T. Noe *et al.*, Nature Phys. **8**, 219 (2012) and J.-H. Kim *et al.*, Sci. Rep. **3**, 3283 (2013)], but its observability conditions have not been fully established. Here, by performing magnetic field (B), temperature (T), and pump power (P) dependent studies of SF intensity, linewidth, and delay time through time-integrated and time-resolved magnetophotoluminescence spectroscopy, we have mapped out the B-T-P region in which SF is observable. In general, SF can be observed only at sufficiently low temperatures, sufficiently high magnetic fields, and sufficiently high laser powers with characteristic threshold behavior. We provide theoretical insights into these behaviors based primarily on considerations on how the growth rate of macroscopic coherence depends on these parameters. These results provide fundamental new insight into electron-hole SF, highlighting the importance of Coulomb interactions among photogenerated carriers as well as various scattering processes that are absent in SF phenomena in atomic and molecular systems.

I. INTRODUCTION

Cooperative emission processes have been studied for a variety of systems since Dicke's seminal theoretical contribution in 1954 [1]. While considering an ensemble of N excited two-level atoms, he found that through the process of photon exchange the radiative decay rate is enhanced by a factor of N and the peak intensity of spontaneous emission (SE) is proportional to N^2, a hallmark of coherent emission. This accelerated radiative decay, or cooperative spontaneous emission, has since been called superradiance (SR) [2–8]. The general concept of SR is widely applicable and has been used to explain radiative coupling of individual oscillators in diverse contexts in the recent literature [9–14].

Here, we consider superfluorescence (SF) [15], which is a cooperative emission process that consists of three clearly defined steps: (i) preparation of an initially incoherent ensemble of excited two-level dipoles; (ii) spontaneous development of macroscopic coherence; and (iii) cooperative radiative decay with coherent light emission. As such, SF is characterized most dramatically by the existence of a finite delay time between the initial excitation and the final emission [16]. In contrast, step (iii) alone would qualify a process to be called SR. Note also that SF is a dissipative process in which the initial energy stored in the population-inverted system is totally converted into light emission; this aspect distinguishes SF from

amplified spontaneous emission (ASE) where at most half of the population inversion is radiated away.

SF has been observed in a number of atomic and molecular systems since the 1970s [17,18]. However, in condensed matter systems, SF has been difficult to observe due to the inherently short coherence times of carriers. Optically created electron-hole (*e-h*) pairs in semiconductors can provide a good system to study many-body physics in a highly controllable environment through magnetic field, temperature, and pair density (laser power). Recently, we observed SF in optically excited InGaAs/GaAs quantum wells by performing pump-probe and time-resolved photoluminescence measurements simultaneously [19]. Many-body renormalization of energies was noted [20], and Coulomb enhancement of gain at the Fermi edge [21] was found to assist cooperative recombination, leading to a novel phenomenon of sequential SF bursts [22]. Overall, it has been established that Coulomb interactions among carriers and continuum of states, unique to solid-state systems, distinguish solid-state SF from atomic SF. However, quantitative understanding of the observability conditions for SF has not been accomplished.

In the present work, we studied SF under a variety of magnetic field (B), temperature (T), and excitation laser power (P) conditions, fully mapping out the region of this three-dimensional parameter space in which SF is observable. We found that SF can be observed only at sufficiently low T, sufficiently high B, and sufficiently high P with characteristic threshold behaviors. For example, for the (11) interband magnetooptical transition, when $B = 17.5$ T and $P = 4$ mW, SF can be observed only when $T < 105$ K; at $B = 17.5$ T and $T = 4$ K, SF can only be induced by excitation power $P > 0.05$ mW. At low B, high T, and low P, SF is replaced by

*Present address: Center for Integrated Nanostructure Physics, Institute for Basic Science, Sungkyunkwan University, Suwon, Republic of Korea.
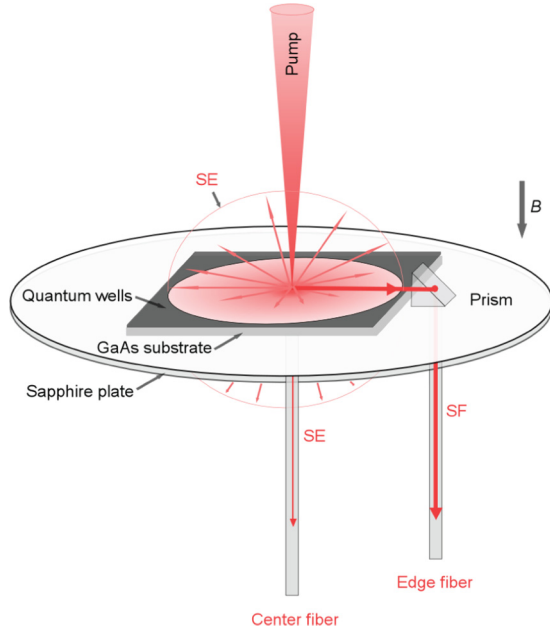
†Corresponding author: kono@rice.edu

FIG. 1. (Color online) Schematic diagram of the experimental geometry. Spontaneous emission (SE) is emitted in all 4π spatial directions while superfluorescence (SF) is emitted in the quantum well plane. A μ prism is placed at one edge of the sample to redirect the in-plane emission (SF) into the edge fiber, while SE is collected through the center fiber placed behind the sapphire plate [23].

SE or ASE. We explain these behaviors by considering how the growth rate of macroscopic coherence depends on these parameters, laying the foundation for the understanding of *e-h* SF in optically excited semiconductors.

II. METHODS

We performed time-integrated photoluminescence (TIPL) and time-resolved photoluminescence (TRPL) spectroscopy experiments at the Ultrafast Optics Facility of the National High Magnetic Field Laboratory (NHMFL) in Tallahassee, Florida. With a 17.5-T superconducting magnet and an amplified Ti:sapphire laser, we performed TIPL and TRPL measurements in the Faraday geometry, where the incident light beam was parallel to the magnetic field and perpendicular to the quantum wells, under various magnetic field, laser power, and temperature conditions.

We used a multiple quantum well sample, grown by molecular beam epitaxy, consisting of 15 layers of 8-nm $In_{0.2}Ga_{0.8}As$ separated by 15-nm GaAs barriers grown on a GaAs buffer layer and GaAs (001) substrate. As shown in Fig. 1, the sample was mounted at the center of a sapphire window, and a micro-prism was located at one edge of the sample to redirect in-plane emission. Two fibers, center and edge fibers, were used for PL collection; the former was used for monitoring SE (which is emitted in all 4π spatial directions with equal probability) while the latter was used to observe SF (which is emitted in the plane of the quantum wells) [19,20,22]. In the SF regime, the emission is strongly directional, propagating along a certain in-plane direction, but the direction changes from shot to shot [23]. TIPL was

measured with a CCD-equipped monochromator, and TRPL was measured using a streak camera system.

The laser system used was an amplified Ti:sapphire laser producing 150 fs pulses of 800 nm (1.55 eV) radiation at a repetition rate of 1 kHz, a small portion of which was used as the optical pump in our experiments. The majority of the beam was used to pump an optical parametric amplifier (OPA), which provided pulsed radiation from UV to 20 μm with appropriate nonlinear crystals. Here, the OPA was used to produce intense outputs with tunable wavelengths between 850 nm and 930 nm. See Refs. [19,20,22–24] for more details about the experimental methods employed.

III. RESULTS AND DISCUSSION

A. Magnetic field dependence

1. Time-integrated PL

Figures 2(a) and 2(b) show the magnetic field dependence of time-integrated center-fiber and edge-fiber-collected PL from 0–10 T under an excitation power of 2 mW and a temperature of 4 K. The most dominant feature in the center-fiber-collected PL in Fig. 2(a) is the lowest energy transition, the $(N_e,N_h) = (00)$ transition in the Landau level (LL) notation (or the $1s$ emission in the 2D hydrogenic notation [25–27]), where N_e (N_h) is the Landau index for the electron (hole). This emission peak slightly blue shifts with increasing magnetic field through the diamagnetic shift [28]. Also, a very weak PL signal can be observed around 1.43 eV and 1.45 eV, which corresponds to the (00) transition of the E_1L_1 and E_2H_2 interband transitions, respectively [27].

In contrast, PL emission detected through the edge fiber increases drastically with the magnetic field, as shown in Fig. 2(b). At zero magnetic field, the edge PL emission spectrum is characterized by two peaks at $\sim$1.32 eV and $\sim$1.43 eV, corresponding to the E_1H_1 $1s$ and E_1L_1 $1s$ transitions, respectively. In addition, continuum emission exists between the two peaks. The shape and intensity of the edge PL spectrum do not sensitively depend on the magnetic field until the magnetic field reaches $\sim$4 T, where LL separation begins to become distinguishable. With further increasing magnetic field, the intensity of the (00) peak increases dramatically, and emission from other LLs also becomes bright. Compared with center PL emission, at high magnetic fields, edge PL emission is much brighter, sharper, and better spectrally separated. As shown in Fig. 2(b), the (00), (11), ..., (99) interband transitions (or $1s$, $2s$, ..., $10s$ transitions in the hydrogenic notation) are clearly observable, all originating from the $B = 0$ T E_1H_1 exciton state. Several other LLs at higher energies are E_1L_1 transitions, which are not relevant to our discussion in the following.

In order to investigate the characteristics of SF emission, we compare the center and edge PL from the (00) LL transition at different magnetic fields, as summarized in Figs. 2(c) and 2(d). In Fig. 2(c), the center PL peak is always broad and does not show much magnetic field dependence while the edge PL peak becomes sharper with increasing magnetic field, especially when the magnetic field is larger than 4 T. In the low-field regime, $B < 4$ T, the linewidth of edge PL stays almost constant around 11 meV, and then it continues to decrease
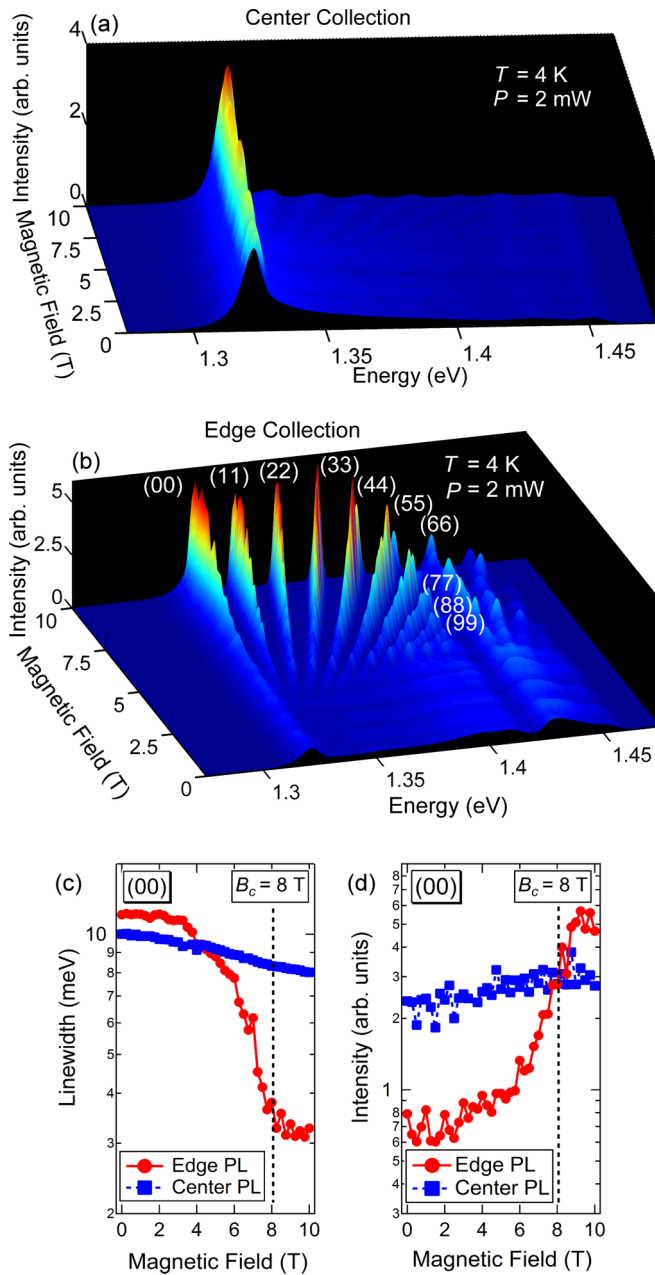
FIG. 2. (Color online) Magnetic field dependence of time-integrated PL collected with the (a) center fiber and (b) edge fiber at 4 K with an average excitation laser power of 2 mW. Magnetic field dependence of the (c) linewidth and (d) intensity of the center and edge collected PL emission of the (00) interband transition.

to ~3 meV at 8 T and stays stable at higher magnetic fields. Therefore, we regard 8 T to be the critical magnetic field, B_c, of SF, i.e., the minimum required magnetic field strength for SF to be observable at this temperature and laser power. Similar behavior is seen in the magnetic field dependence of the PL peak intensity in the edge case, as shown in Fig. 2(d). In the SF regime, the edge PL intensity becomes nearly constant. In contrast, the center PL intensity only slightly increases with the magnetic field.

2. Time-resolved PL

Figure 3 shows time-resolved observations of SF bursts at different magnetic fields from 0–10 T at a temperature of 4 K and excitation power of 2 mW. At each magnetic field, a series of SF bursts is observed, with longer delay times at lower photon energies, consistent with the previously observed sequential SF behavior [20,22]. At low magnetic fields, continuous SF emission occurs in the whole spectral regime except a slight kink around the energy corresponding to the E_1L_1 band edge. One thing worth highlighting here is that the heavy-hole band-edge PL at zero magnetic field, or the (00) emission at a finite magnetic field, is strong in the time-integrated PL spectra as shown in Fig. 2(b) but weak in the time-resolved PL emission as shown in Fig. 3. These differences are real, because the heavy-hole band-edge PL at zero magnetic field, or the (00) emission at a finite magnetic field, comes not only from coherent bursts but also from spontaneous emission. The latter lasts for a long time (up to a nanosecond) and thus accumulates to become a dominant feature in time-integrated PL spectra.

With increasing magnetic field up to 6 T, some discrete bursts with small amplitudes appear as wiggles on the continuous emission background. When the magnetic field is higher than 6 T, strong bursts of SF emission, discrete both in time and energy, are observed. Figure 4 summarizes the pulse time delay as a function of magnetic field for different (N_e, N_h) transitions. Higher LLs have shorter delay times, as noted above, and for each (N_e, N_h) transition, the pulse time delay decreases with increasing magnetic field.

3. Discussion

In general, a high magnetic field is expected to make SF observation easier since Landau quantization in a two-dimensional quantum well structure will enhance gain and increase the coherence time by reducing the phase space available for scattering. When the carrier concentration is low enough, the gain increase is mainly due to an enhanced density of states and overlap of electron and hole wave functions in a two-body excitonic state [19,29]. For example, when the magnetic field increases from 0.1 to 17 T, the excitonic enhancement $|R_m(0)|$ of the interband dipole matrix element increases by a factor of 1.4 for (00) emission, 4.6 for (11) emission, and 7.9 for (22) emission, see Fig. 5. For the definition of $R_m(0)$, see Refs. [19] and [30]. The gain scales as a square of this factor. At high carrier densities the main effect is the many-body enhancement of the gain just below the Fermi edge. As was shown in Fig. 5 of Ref. [22], the peak gain increases by a factor of 20 when the magnetic field increases from 0–17 T. All these factors would make the SF observability conditions easier to satisfy, generally consistent with our experimental results.

Figure 2 shows that strong SF emission appears only in the edge collection while the center collection only shows ordinary spontaneous emission, which clearly confirms the importance of gain in the SF emission process. In this sample, optical gain exists only for electromagnetic waves propagating along the quantum well plane, which leads to in-plane SF emission; no optical gain is available in the direction perpendicular to the
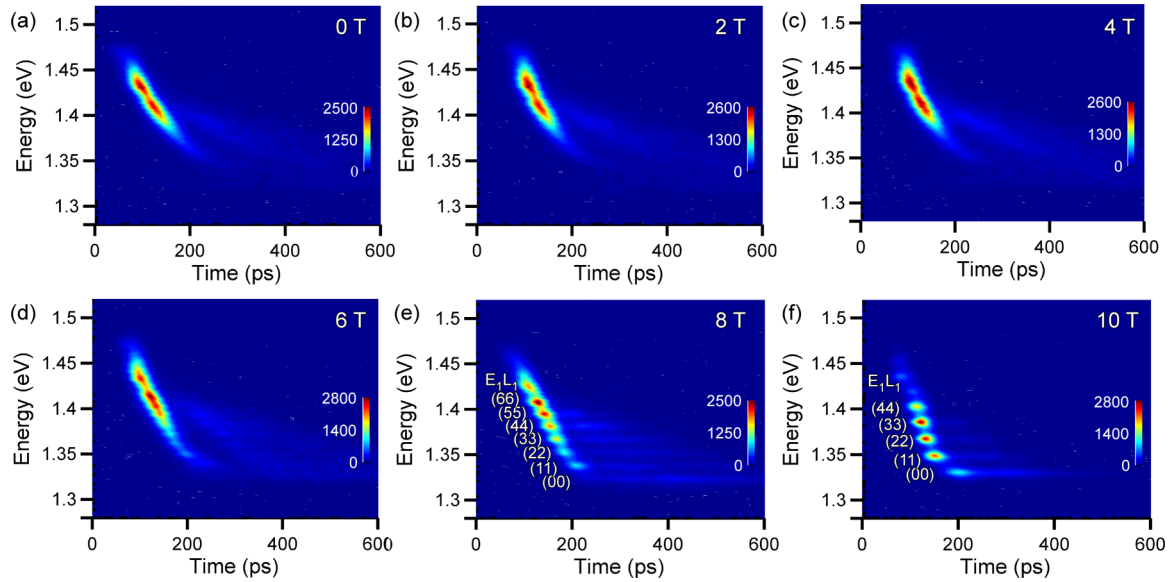
FIG. 3. (Color online) Color surface plots of time-resolved photoluminescence spectra at different magnetic fields at a temperature of 4 K and an excitation laser power of 2 mW. Here, the time 'zero' on the time axis corresponds to the laser pulse excitation time when the *e-h* pairs are created. See Supplemental Material for more information [31].

sample plane, leading to ordinary spontaneous emission in the center collection.

With increasing magnetic field, the edge (00) emission goes through several different emission stages: at $B < 4$ T, the intensity and linewidth stay constant with increasing magnetic field, just as the emission feature from the center PL. This suggests that in (00) emission spontaneous emission dominates in this low magnetic field regime, and the *e-h* dipoles are incoherent, radiating independently from each other through spontaneous recombination. When the magnetic field is larger than 4 T, the linewidth of the edge emission gradually decreases due to the gain narrowing effect in the ASE process, during which the frequency components near the peak in the gain spectrum are preferentially amplified and the emission strength becomes larger. When the magnetic field further increases up to 8 T, the linewidth decreases to around 3 meV, and stays constant with increasing magnetic field while the intensity

becomes much larger than that in the spontaneous emission process and eventually saturates. The saturation of linewidth is a characteristic feature of SF caused by the pulse shortening below the dephasing time, so that the linewidth is controlled by the growth rate of the field instead of incoherent scattering processes [6,32]. Moreover, with increasing growth rate and decreasing SF pulse duration the linewidth of SF emission is expected to grow, although this behavior would be possible to see only in measurements resolving individual pulses. The time-integrated intensity gets saturated after stimulated recombination from higher LLs becomes efficient enough to consume photoexcited *e-h* pairs before they reach the (00) LL.

At a temperature of 4 K and excitation power of 2 mW, a minimum magnetic field of ~8 T is found to be the
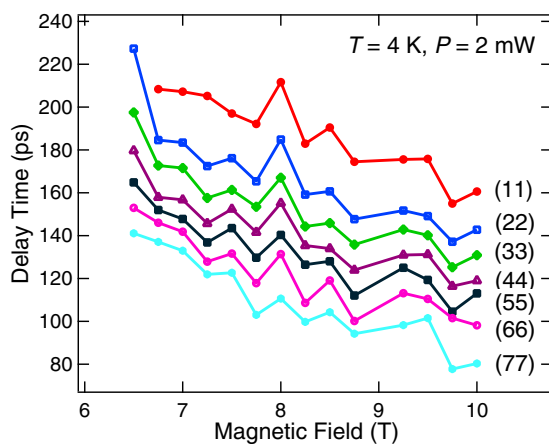

FIG. 4. (Color online) Magnetic field dependence of SF delay time for different (N_e, N_h) transitions at 4 K and 2 mW.
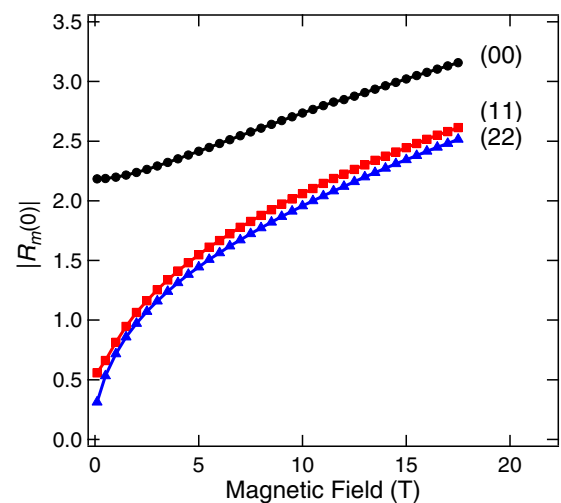

FIG. 5. (Color online) The magnetic field dependence of the excitonic enhancement $|R_m(0)|$ of the interband dipole matrix element for different Landau levels.

critical magnetic field for the appearance of SF. Above this critical magnetic field, the growth rate of a macroscopic polarization is faster than the dephasing rate, and cooperative SF emission occurs. This critical magnetic field is a function of temperature and excitation power, becoming smaller with decreasing temperature and increasing excitation power.

From the magnetic field dependence of time-resolved PL in Fig. 4, it can be seen that the delay time for any transition generally decreases with the magnetic field, which means that a higher magnetic field would induce an earlier appearance of SF emission. This behavior is consistent with our expectation that a high magnetic field makes the development of macroscopic coherence faster. When comparing the delay times of different transitions, we notice that a higher energy level has a shorter pulse time delay, i.e., faster growth rate of SF emission. To understand this behavior, we need to consider the Coulomb interactions between electrons and holes in this e-h system. The Coulomb interactions can increase the gain at the quasi-Fermi edge [21,22], resulting in the highest gain for the LL just below the quasi-Fermi edge [22]. Therefore, the electrons and holes in the higher energy levels recombine first, followed by a series of sequential SF bursts at lower and lower energy levels as the quasi-Fermi energy decreases due to recombination of carriers.

B. Temperature dependence

1. Time-integrated PL

Figure 6(a) shows the temperature dependence of the edge PL spectrum from 4 K to 160 K at $B = 17.5$ T with an excitation power of 4 mW. The (00), (11), and (22) emission peaks originating from E_1H_1 and a few peaks from E_1L_1 are observed. The emission peaks are strong and sharp at low temperatures but gradually become weaker and broader with increasing temperature. Also, all the peaks red shift with increasing temperature because the band gap shrinks with the temperature [33]. At $T > 100$ K, the (00) emission peak vanishes first, which is followed by the (11) and (22) peaks.

To see the strong temperature dependence more clearly, (11) emission spectra at different temperatures are shown in Fig. 6(b). A clear transition is seen from sharp and bright emission at low temperatures to broad and weak emission at high temperatures. Note that the 160 K spectrum is multiplied by a factor of 144 to show it on the same scale as the spectra at low temperatures. By analyzing the intensity and linewidth of the (11) emission as shown in Fig. 6(c), a critical temperature, T_c, of 105 K is obtained. Below this temperature, SF emission is observable. The value of T_c is a function of magnetic field and laser excitation power; it also depends on from which (N_e,N_h) transition the SF emission originates.

2. Time-resolved PL

Figure 7 shows the temperature dependence of SF bursts at 10 T and 2 mW. At each temperature, we can see multiple SF bursts from different LLs with delay times that are shorter for higher LLs. With increasing temperature, the intensity of SF bursts gradually decreases, and finally, at $T > 150$ K, no SF bursts can be observed, consistent with the time-integrated PL results (Sec. III B 1). Figure 8(a) plots
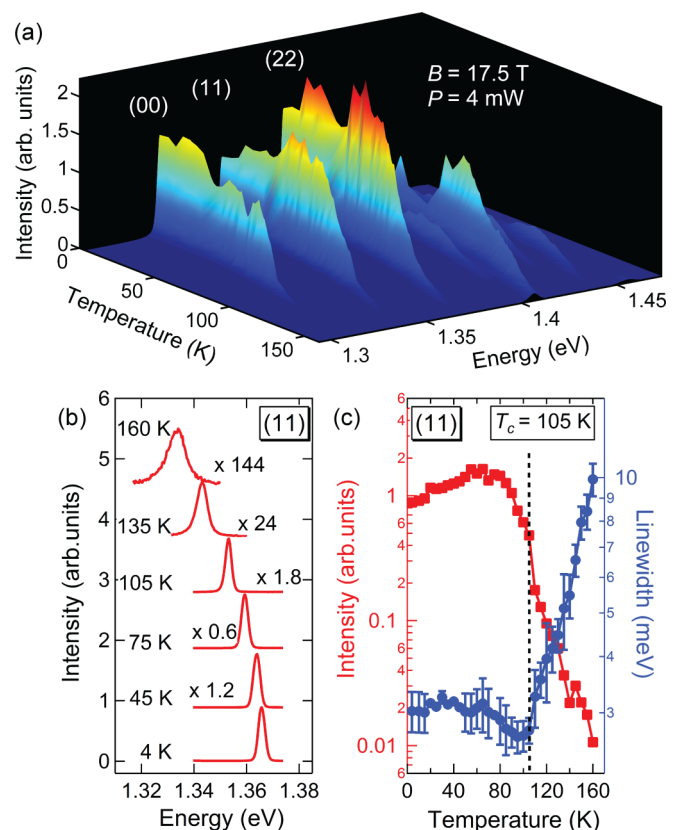

FIG. 6. (Color online) (a) Temperature dependence of time-integrated PL collected through the edge fiber at 17.5 T with an excitation power of 4 mW. (b) Emission spectra of the (11) transition at different temperatures. (c) The linewidth and intensity of the (11) emission as a function of temperature.

the temperature dependence of SF delay times for different (N_e,N_h) transitions. The delay time increases monotonically with increasing temperature for all peaks except the (00) peak. Figure 8(b) shows the temperature dependence of integrated intensities for different (N_e,N_h) transitions, showing that SF vanishes at high temperatures, again consistent with results of TRPL.

3. Discussion

SF is easier to observe at lower temperatures, where the dephasing rate can be greatly suppressed leading to longer coherence time, T_2. At higher temperatures, many mechanisms can destroy the coherent state, among which the electron-phonon scattering is dominant. Therefore, the SF observability condition that the cooperative frequency should be larger than the dephasing rate [29] is not easily satisfied at high temperatures. In addition, high temperature would broaden the quasi-Fermi edge of the Fermi-Dirac distribution, destroying the quantum degeneracy condition, necessary for gain enhancement at the Fermi-edge in an e-h system. These expectations are generally consistent with our temperature-dependent observations of SF.

More quantitatively, Fig. 6 shows that SF bursts originating from E_1H_1 are only sharp and strong in the low-temperature regime, i.e., $T < 100$ K, and suddenly disappear at high
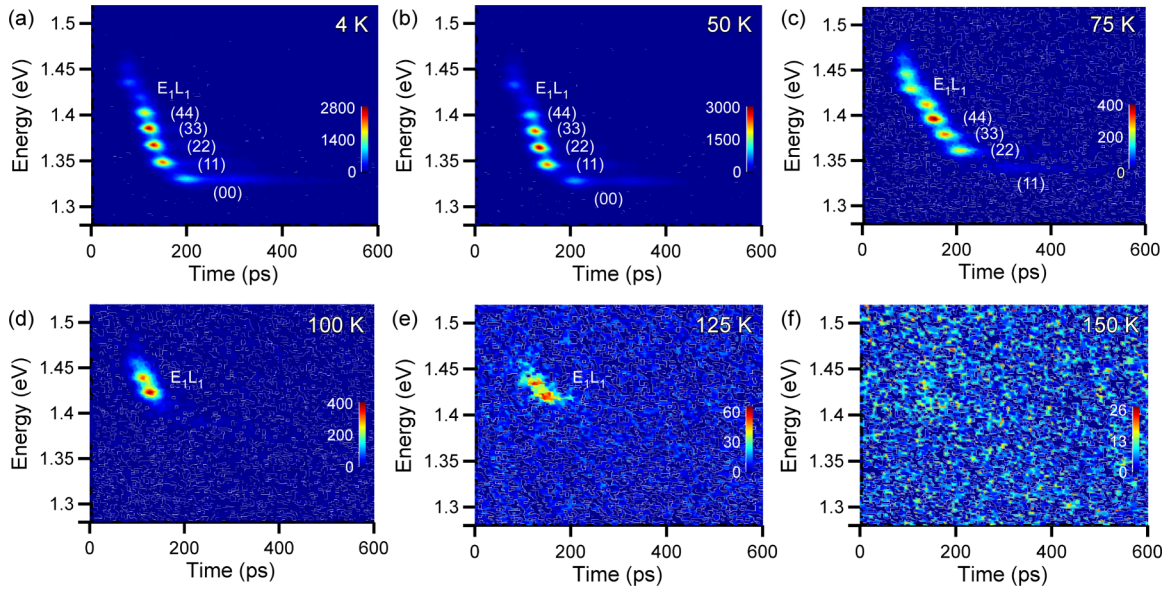
FIG. 7. (Color online) Color surface plots of time-resolved photoluminescence spectra at different temperatures at a magnetic field of 10 T and an excitation laser power of 2 mW.

temperatures. This time-integrated PL result agrees well with the time-resolved emission feature in Fig. 7, which shows that no clear emission can be observed from the lower LLs at $T > 100$ K. From the linewidth and intensity analysis in Figs. 6(b) and 6(c), the effect of temperature on SF observation is even clearer. For both the (00) and (11) transitions, the linewidth stays constant at low temperatures, as it is controlled by the SF dynamics. As the temperature increases, phonon relaxation is activated and the coherence between e-h dipole oscillations gets destroyed by dephasing. The latter process starts controlling the linewidth and causes its sharp increase with increasing temperature. The emission intensity sharply drops at the same time: by more than a factor of 200 between 100 K and 160 K. Therefore, the critical temperature can be defined as the turning point where the intensity begins to drop and the linewidth starts increasing. This critical temperature is higher for higher LLs because of a larger gain, which moves

the SF threshold to higher temperatures and dephasing rates. Also, this critical temperature for the onset of SF emission is a function of magnetic field and excitation power, becoming higher with increasing magnetic field and laser excitation power.

From the time-resolved emission results, one can see the similar effect of temperature on the pulse time delay. For each transition, the delay time increases with increasing temperature because of the decreasing growth rate of the optical polarization and the field. The delay time is larger for lower-energy transitions, resulting in the sequential nature of SF bursts, which can be again understood by the enhanced gain at the Fermi edge induced by the Coulomb interactions between electrons and holes [22].

C. Excitation laser power dependence

1. Time-integrated PL

Figure 9(a) shows the laser excitation power dependence of edge-fiber-collected emission from an average power of 2 μW to 7 mW at $B = 17.5$ T and $T = 4$ K. With increasing laser power, bright and sharp emission lines appear around 100 μW and grow in intensity rapidly and eventually tend to saturate in the highest power regime. Figure 9(b) shows (11) emission spectra taken with various excitation powers. With an excitation power of 8 μW, the (11) peak is not observable. Figures 9(c) and 9(d) show the linewidth and intensity of the (11) peak as a function of laser power in Fig. 9(c) log scale and Fig. 9(d) linear scale. From Fig. 9(c), we can determine the critical laser power, P_c, to be 50 μW for SF appearance for the (11) transition. In Fig. 9(d), the saturation behavior at high laser powers is seen more clearly.

In order to estimate the density of e-h pairs, n_{pair}, under different excitation powers, P, we use the degeneracy, $g_{LL}[\text{cm}^{-2}] = 2eB/h = 4.8 \times 10^{10} \times B$ of each Landau level at magnetic field B [T], including the twofold spin degeneracy. At a magnetic field of 17.5 T, a minimum power of 10 μW
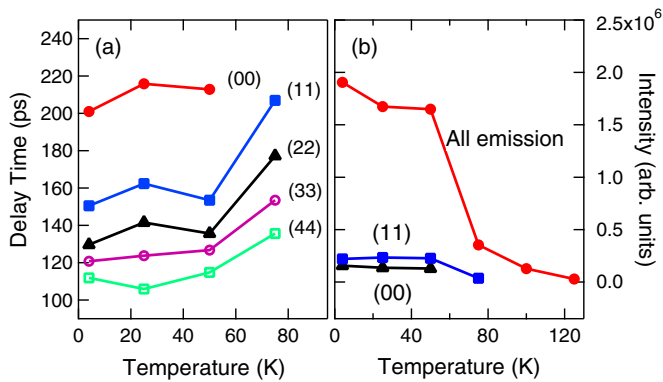

FIG. 8. (Color online) (a) Temperature dependence of SF delay times for different (N_e, N_h) at 10 T and 2 mW. (b) Temperature dependence of spectrally and temporally integrated peak intensities at 10 T and 2 mW for all emission peaks, the (00) peak and the (11) peak.
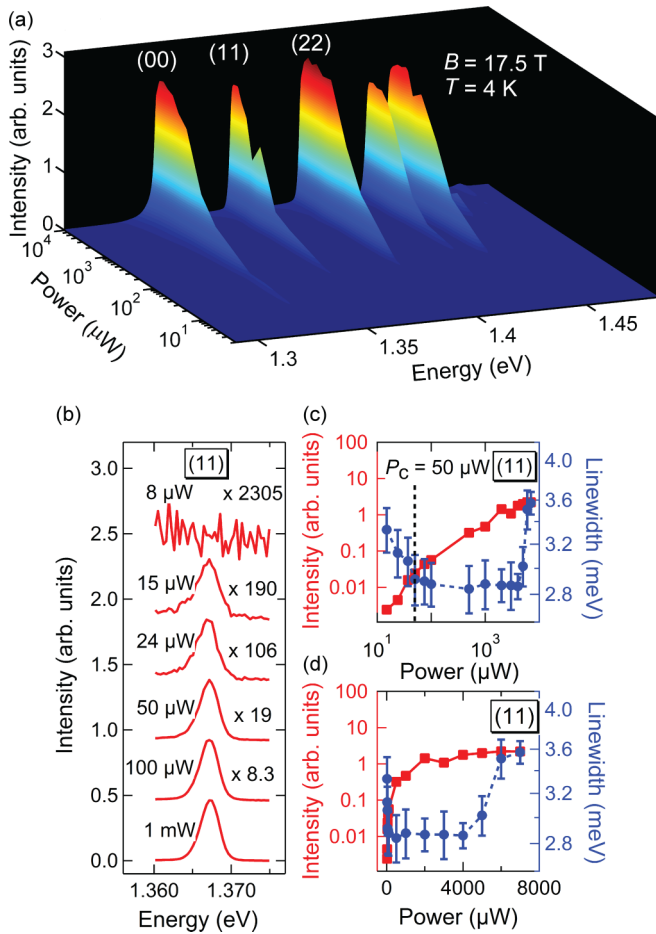
FIG. 9. (Color online) (a) Excitation laser power dependence of time-integrated edge PL spectra at 17.5 T and 4 K. (b) (11) emission spectra with different laser excitation powers at 17.5 T and 4 K. (c)–(d) The linewidth and intensity of the (11) emission as a function of average excitation laser power in (c) log scale and (d) linear scale.

was needed for the appearance of emission from the (11) transition, which, we interpret, corresponds to the situation that the (00) Landau level has just been filled completely. Similarly, a power of ∼20 μW was necessary for the appearance of emission from the (22) transition, which, we interpret, corresponds to the situation that the (00) and (11) Landau levels have just been filled completely. These observations allow us to assume the following linear relationship between the *e-h* pair density and laser power in this low-power regime: n_{pair} [cm^{-2}] $= 8.5 \times 10^{10} \times P$ [μW]. At higher laser powers, saturation occurs, and this relationship breaks down.

2. Time-resolved PL

Figure 10 shows SF bursts excited with different laser powers at 17.5 T and 4 K. At low excitation powers, such as 0.25 mW, only the SF burst through the (00) transition can be observed, and SF from the (11) transition appears when the power increases to 0.5 mW. When the power is larger than 0.75 mW, 4 SF bursts—(00), (11), (22), and E_1L_1—can be observed. Figure 11 shows the power dependence of SF intensity and delay time at different magnetic fields for different transitions. For a given magnetic field, the power dependence is qualitatively the same for all transitions, but the trend is qualitatively different at different magnetic fields. Most dramatically, the delay time generally decreases with increasing power at 0 T but monotonically increases with increasing power at 17.5 T.

3. Discussion

Since SF develops under the conditions of high gain, it is generally anticipated that it should have a certain excitation power threshold. With increasing excitation fluence, the edge emission from a given LL develops from spontaneous emission to ASE when the electron degeneracy is reached, and finally to SF.
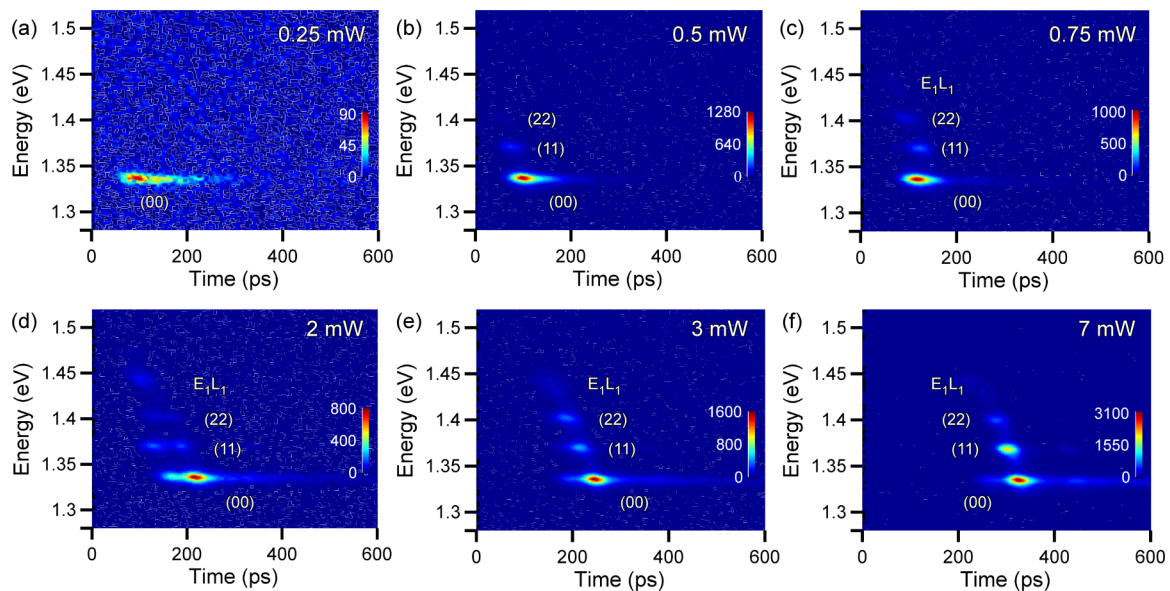

FIG. 10. (Color online) Color surface plots of time-resolved photoluminescence spectra at different excitation laser powers at a magnetic field of 17.5 T and a temperature of 4 K.
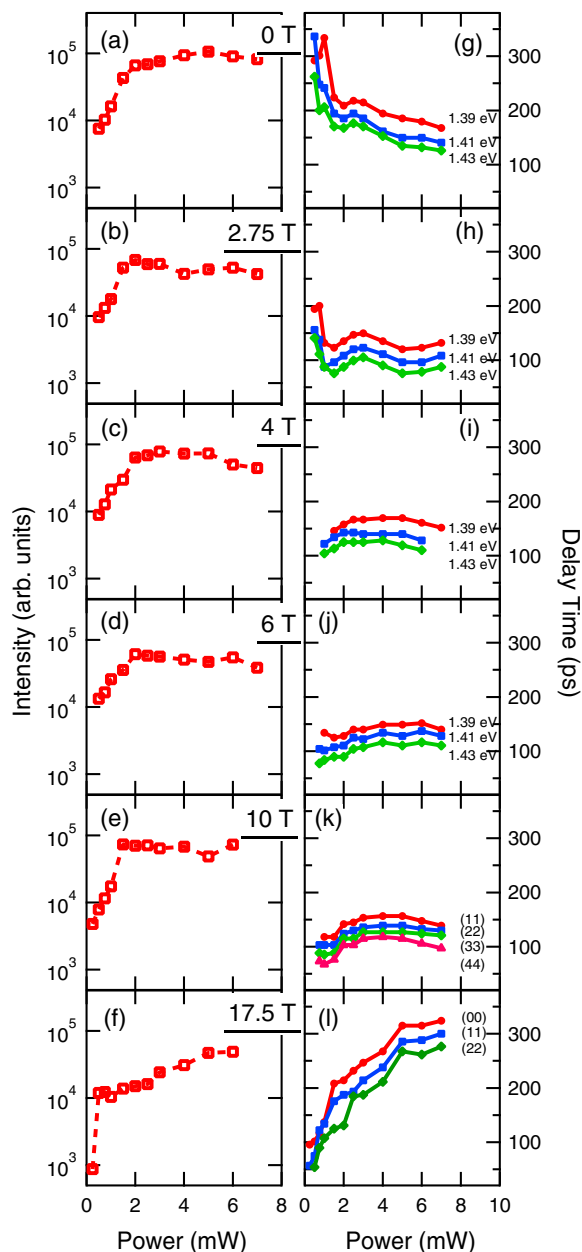
FIG. 11. (Color online) (a)–(f): Power dependence of spectrally and temporally integrated emission intensity at different magnetic fields at 4 K, showing saturation behavior at high powers. (g)–(l): Power dependence of delay times at different magnetic fields for different (N_e, N_h) peaks at 4 K.

Figure 9(a) clearly shows that strong and sharp stimulated emission can only be observed at high excitation powers, i.e., high *e-h* pair density. At a low power level such as 8 μW shown in Fig. 9(b), no emission can be observed in the edge collection. At the same time, we can still see clear spontaneous emission from the center collection (not shown). This shows that no optical gain is available in the system. With increasing excitation power, optical gain begins to appear in the system, and stimulated emission is detected through the edge fiber. As the excitation power further increases, the growth rate of the field becomes high enough to exceed the dephasing rate and SF emission develops. The linewidth initially drops

with increasing pump intensity and gets saturated once SF becomes dominant, its growth rate controlling the linewidth. The increase of linewidth at highest intensities could be related to the SF pulse shortening. However, this is impossible to verify based on time-integrated data. One would have to measure spectra of individual SF pulses, which is not feasible. The time-integrated intensity gets saturated as photoexcited carriers occupying all states at a given LL are consumed by stimulated recombination with high efficiency. So a critical power, corresponding to a critical *e-h* pair density, for SF observation can be determined based on the linewidth and intensity behavior. This critical excitation power is a function of magnetic field and temperature, becoming lower with increasing magnetic field and decreasing temperature.

The effect of excitation power, corresponding to a certain *e-h* pair density, on state filling is clearly seen in the time-resolved PL results presented in Fig. 10. When the power is at 0.25 mW, only the lowest (00) transition can be observed, and this emission has a tail lasting for around 200 ps. This long emission tail is a signature of spontaneous emission, i.e., the emission is incoherent. When the power is increased to 0.5 mW, an emission peak appears through the (11) transition since more electrons and holes are available to fill the higher energy level. With further increasing excitation power, more and more Landau levels are filled and emissions appear in a broad spectrum range.

The SF pulse delay time shows an interesting dependence on the excitation power, i.e., the *e-h* pair density, at different magnetic fields, shown in Fig. 11. At zero magnetic field, the delay time generally decreases with increasing power, consistent with the expectation that the macroscopic polarization can be built faster with more *e-h* pairs, inducing earlier appearance of emission. However, at high magnetic fields, the delay time increases with increasing laser power. Also at high excitation powers the delay increases with the magnetic field. One possible reason is that the strong magnetic field slows down the time it takes carriers to relax to the lowest LLs and quasithermalize, i.e., reach the degenerate distribution. With increasing excitation power the temperature of the initial electron distribution increases, thus leading to longer cooling times.

D. *B-T-P* diagram of SF

As stated above, experimentally, there are three parameters that cooperatively determine whether SF can be observed, i.e., magnetic field (B), temperature (T), and laser power (P), the last of which is related to the *e-h* pair density (n_{pair}). With increasing magnetic field, SF can be observed at higher temperatures and lower laser power. When the dependence of SF on these three parameters is fully mapped out, a phase diagram can be constructed, showing under what conditions SF emission can appear, as shown in Figs. 12(a) and 12(b).

Figure 12(a) shows the *B-P* phase diagram at 4 K for the (11) transition. The critical power, P_c, corresponding to the critical *e-h* pair density for SF observation, decreases with increasing B. Strikingly, with increasing B, P_c decreases exponentially, down to the μW level at the highest B, corresponding to n_{pair} on the level of 10^{12} cm^{-2}. This suggests that the exponential suppression of the dephasing rate with
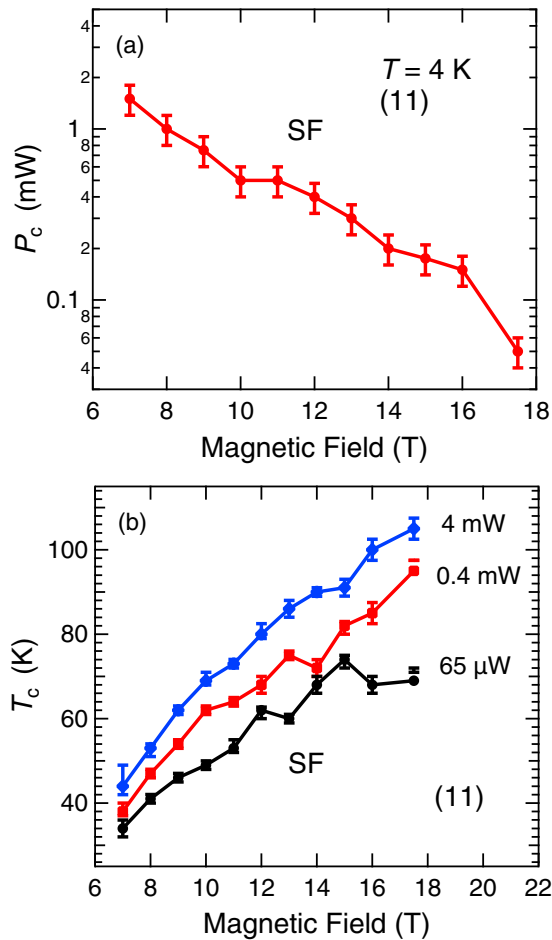
FIG. 12. (Color online) (a) Magnetic field dependence of the critical laser power, P_c, of SF for the (11) transition at 4 K. (b) Magnetic field dependence of the critical temperature, T_c, of SF under different excitation powers for the (11) transition.

magnetic field due to opening the gaps in the density of states between the LLs is the main mechanism in lowering the SF threshold.

Figure 12(b) shows the B-T_c phase diagram at different excitation powers for the (11) transition. The temperature T_c at the SF threshold increases with B monotonically and the dependence is close to linear, again in agreement with the scaling of the dephasing rate $\propto \exp(-\frac{\Delta}{k_B T})$, where $\Delta \propto B$ is the energy distance between adjacent Landau levels. Also, with a higher laser excitation power, SF can be observed at higher temperatures and lower magnetic fields.

IV. CONCLUSIONS

We used time-integrated and time-resolved photoluminescence spectroscopy to investigate superfluorescence emission from semiconductor quantum wells in the spectral and time domains under different magnetic field, temperature, and laser excitation power conditions, and successfully mapped out the B-T-P phase diagram of SF emission. The temperature, magnetic field, and excitation laser power corresponding to the SF threshold for each (N_e, N_h) transition determine a surface in the B-T-P space, which separates the SF regime at low temperatures, high magnetic fields, and high excitation powers from the spontaneous emission and amplified spontaneous emission regimes. The transition between ASE and SF regimes is marked by distinct changes in the edge emission intensity and linewidth. These results thus lay the foundation for refining our understanding of cooperative emission processes and nonequilibrium many-body dynamics in optically created electron-hole systems.

[1] R. H. Dicke, Phys. Rev. **93**, 99 (1954).

[2] N. E. Rehler and J. H. Eberly, Phys. Rev. A **3**, 1735 (1971).

[3] A. V. Andreev, V. I. Emel'yanov, and Y. A. Il'inskii, Sov. Phys. Usp. **23**, 493 (1980).

[4] M. Gross and S. Haroche, Phys. Rep. **93**, 301 (1982).

[5] H. Haken, *Laser Theory* (Springer, Berlin, 1984).

[6] V. V. Zheleznyakov, V. V. Kocharovsky, and VI. V. Kocharovsky, Sov. Phys. Usp. **32**, 835 (1989).

[7] A. A. Belyanin, V. V. Kocharovsky, and VI. V. Kocharovsky, Solid State Commun. **80**, 243 (1991).

[8] M. O. Scully and A. A. Svidzinsky, Science **325**, 1510 (2009).

[9] J. G. Bohnet, Z. Chen, J. M. Weiner, D. Meiser, M. J. Holland, and J. K. Thompson, Nature (London) **484**, 78 (2012).

[10] K. Baumann, C. Guerlin, F. Brennecke, and T. Esslinger, Nature (London) **464**, 1301 (2010).

[11] D. Martín-Cano, L. Martín-Moreno, F. J. García-Vidal, and E. Moreno, Nano Lett. **10**, 3129 (2010).

[12] M. Scheibner, T. Schmidt, L. Worschech, A. Forchel, G. Bacher, T. Passow, and D. Hommel, Nature Phys. **3**, 106 (2007).

[13] L. Ren, Q. Zhang, C. L. Pint, A. K. Wójcik, M. Bunney, T. Arikawa, I. Kawayama, M. Tonouchi, R. H. Hauge, A. A. Belyanin, and J. Kono, Phys. Rev. B **87**, 161401(R) (2013).

[14] Q. Zhang, T. Arikawa, E. Kato, J. L. Reno, W. Pan, J. D. Watson, M. J. Manfra, M. A. Zudov, M. Tokman, M. Erukhimova, A. A. Belyanin, and J. Kono, Phys. Rev. Lett. **113**, 047601 (2014).

[15] R. Bonifacio and L. A. Lugiato, Phys. Rev. A **11**, 1507 (1975).

[16] Q. H. F. Vrehen and H. M. Gibbs, in *Dissipative Systems in Quantum Optics*, Topics in Current Physics, edited by R. Bonifacio (Springer-Verlag, Berlin, 1982), Chap. 6, pp. 111–147.

[17] N. Skribanowitz, I. P. Herman, J. C. MacGillivray, and M. S. Feld, Phys. Rev. Lett. **30**, 309 (1973).

[18] H. M. Gibbs, Q. H. F. Vrehen, and H. M. J. Hikspoors, Phys. Rev. Lett. **39**, 547 (1977).

[19] G. T. Noe II, J.-H. Kim, J. Lee, Y. Wang, A. K. Wojcik, S. A. McGill, D. H. Reitze, A. A. Belyanin, and J. Kono, Nature Phys. **8**, 219 (2012).

[20] J.-H. Kim, J. Lee, G. T. Noe, Y. Wang, A. K. Wójcik, S. A. McGill, D. H. Reitze, A. A. Belyanin, and J. Kono, Phys. Rev. B **87**, 045304 (2013).

[21] S. Schmitt-Rink, C. Ell, and H. Haug, Phys. Rev. B **33**, 1183 (1986).

[22] J.-H. Kim, G. T. Noe II, S. A. McGill, Y. Wang, A. K. Wójcik, A. A. Belyanin, and J. Kono, Sci. Rep. **3**, 3283 (2013).

[23] Y. D. Jho, X. Wang, J. Kono, D. H. Reitze, X. Wei, A. A. Belyanin, V. V. Kocharovsky, VI, V. Kocharovsky, and G. S. Solomon, Phys. Rev. Lett. **96**, 237401 (2006).

[24] G. T. Noe II, J.-H. Kim, J. Lee, Y.-D. Jho, Y. Wang, A. K. Wójcik, S. A. McGill, D. H. Reitze, A. A. Belyanin, and J. Kono, Fortschr. Phys. **61**, 393 (2013).

[25] A. H. MacDonald and D. S. Ritchie, Phys. Rev. B **33**, 8336 (1986).

[26] G. E. W. Bauer and T. Ando, Phys. Rev. B **38**, 6015 (1988).

[27] Y. D. Jho, F. V. Kyrychenko, J. Kono, X. Wei, S. A. Crooker, G. D. Sanders, D. H. Reitze, C. J. Stanton, and G. S. Solomon, Phys. Rev. B **72**, 045340 (2005).

[28] O. Akimoto and H. Hasegawa, J. Phys. Soc. Jpn. **22**, 181 (1967).

[29] Y. D. Jho, X. Wang, D. H. Reitze, J. Kono, A. A. Belyanin, V. V. Kocharovsky, VI. V. Kocharovsky, and G. S. Solomon, Phys. Rev. B **81**, 155314 (2010).

[30] H. Haug and S. W. Koch, *Quantum Theory of the Optical and Electronic Properties of Semiconductors* (World Scientific, Singapore, 2009).

[31] See Supplemental Material at http://link.aps.org/supplemental/10.1103/PhysRevB.91.235448 for a detailed magnetic field dependence of time-resolved photoluminescence spectra at a temperature of 4 K and an excitation laser power of 2 mW.

[32] A. A. Belyanin, V. V. Kocharovsky, and VI. V. Kocharovsky, Quantum Semiclass. Opt. (JEOS, Part B) **9**, 1 (1997).

[33] Y. P. Varshni, Physica **34**, 149 (1967).